

## Article

# Probing the Lorentz Invariance Violation via Gravitational Lensing and Analytical Eigenmodes of Perturbed Slowly Rotating Bumblebee Black Holes

Mert Mangut <sup>1,\*</sup>, Huriye Gürsel <sup>1,†</sup>, Sara Kanzi <sup>2,†</sup> and İzzet Sakallı <sup>1,†</sup>

<sup>1</sup> Department of Physics, Eastern Mediterranean University, North Cyprus via Mersin 10, Famagusta 99628, Turkey; huriye.gursel@emu.edu.tr (H.G.); izzet.sakalli@emu.edu.tr (İ.S.)

<sup>2</sup> Faculty of Engineering, Final International University, North Cyprus via Mersin 10, Kyrenia 99370, Turkey; sara.kanzi@final.edu.tr

\* Correspondence: mert.mangut@emu.edu.tr

† These authors contributed equally to this work.

**Abstract:** The ability of bumblebee gravity models to explain dark energy, which is the phenomenon responsible for the universe's observed accelerated expansion, is one of their most significant applications. An effect that causes faster expansion can be linked to how much the Lorentz symmetry of our universe is violated. Moreover, since we do not know what generates dark energy, the bumblebee gravity theory seems highly plausible. By utilizing the physical changes happening around a rotating bumblebee black hole (RBBH), we aim to obtain more specific details about the bumblebee black hole's spacetime and our universe. However, as researched in the literature, slow-spinning RBBH (SRBBH) spacetime, which has a higher accuracy, will be considered instead of general RBBH. To this end, we first employ the Rindler–Ishak method (RIM), which enables us to study how light is bent in the vicinity of a gravitational lens. We evaluate the deflection angle of null geodesics in the equatorial plane of the SRBBH spacetime. Then, we use astrophysical data to see the effect of the Lorentz symmetry breaking (LSB) parameter on the bending angle of light for numerous astrophysical stars and black holes. We also acquire the analytical greybody factors (GFs) and quasinormal modes (QNMs) of the SRBBH. Finally, we visualize and discuss the results obtained in the conclusion section.

**Keywords:** bumblebee gravity theory; gravitational lensing; black holes; quasinormal modes; Lorentz symmetry breaking; greybody factors



**Citation:** Mangut, M.; Gürsel, H.; Kanzi, S.; Sakallı, İ. Probing the Lorentz Invariance Violation via Gravitational Lensing and Analytical Eigenmodes of Perturbed Slowly Rotating Bumblebee Black Holes. *Universe* **2023**, *9*, 225. <https://doi.org/10.3390/universe9050225>

Academic Editors: Eugeniu Mihnea Popescu and Lucia Aurelia Popa

Received: 28 March 2023

Revised: 9 May 2023

Accepted: 10 May 2023

Published: 12 May 2023



**Copyright:** © 2023 by the authors. Licensee MDPI, Basel, Switzerland. This article is an open access article distributed under the terms and conditions of the Creative Commons Attribution (CC BY) license (<https://creativecommons.org/licenses/by/4.0/>).

## 1. Introduction

The study of the Lorentz invariance [1], a fundamental principle in Einstein's theory of general relativity, has been a topic of great interest in the scientific community. The Lorentz invariance states that the laws of physics are the same for all observers, regardless of the relative motion. In recent years, various experimental and theoretical attempts have been made to test the validity of this principle, and possible violations have been suggested [2–6]. While we acknowledge that there are many studies [7–10] that discuss the effect of quantum gravity on black holes, our study focuses specifically on the effect of the Lorentz invariance violation (LIV) on the properties of black holes.

The bumblebee gravity theory [11,12] is a modification of general relativity that includes a non-zero scalar field, also known as the “bumblebee field”. This field allows for the LIV [13–15], and has been proposed as a way to explore possible deviations from the standard model of physics [16,17]. One of the earliest studies on the bumblebee gravity theory was introduced as a toy model by Kostelecky et al. [2,18–20] and by Bertolami and Paramos [21], who derived the vacuum solutions of a bumblebee gravity model with vector-induced spontaneous LSB. This was followed by a series of papers [5,22–38] that

investigated various aspects of bumblebee gravity, including its effects on the early universe and gravitational lensing, its relation to dark energy, its implications for gravitational waves and thermal radiation, and new black hole and wormhole solutions. In particular, in recent years, there has been growing interest in the studies of bumblebee black holes [39], which are solutions to the field equations of bumblebee gravity. Casana et al. [22] initially reported an almost Schwarzschild spacetime solution using the bumblebee model, with the bumblebee field having only a radial component. Very recently, Xu et al. [40] significantly extended Casana et al.'s static solution and discovered spherical solutions with a temporal component of the bumblebee field. The kinetic term seen in the action [40] has suggested that the radial component is non-dynamic and can be removed from the field equations. They found two families of solutions, one from a set of two second-order differential equations and another from a set of three. The temporal component of the bumblebee field is crucial for both families of solutions as it dramatically changes the behavior of the metric near the black hole event horizon. Remarkably, it enables the existence of solutions with a non-vanishing  $g_{tt}$  at the event horizon. The static bumblebee black hole solutions have been followed by RBBH studies [25,28,41–43], which account for rotation. In those spinning bumblebee gravity models, the gravitational field is described by a metric that includes cross-diagonal terms that are associated with the rotation of the black hole. The field equations are also modified to account for rotation, resulting in a more complex set of equations [27]. However, studies on RBBH have gained momentum in recent years. The first RRBH solution was found in 2019 by Ding et al. [25], who showed that the bumblebee field can impact the properties of rotating black holes, including their shapes, sizes, and gravitational attraction. This was followed by several other studies that investigated the effects of rotation on bumblebee black holes, including their QNMs, GFs, shadow, superradiant instability, and many other features [5,23,28,29,32,34,36,44–50]. These studies have shed new light on the properties and behaviors of bumblebee black holes and their potential implications for our understanding of the universe. On the other hand, gravitational lensing (the bending of light due to the gravitational attraction of massive objects), GFs (factors that describe how the emission spectrum of the black hole differs from a completely uniform black-body spectrum), and QNMs (characteristic ringing patterns produced by black holes after disturbances) are promising methods for probing the LIV effects.

Gravitational lensing is a fascinating phenomenon in which the path of light is bent by the gravitational force of a massive object, such as a galaxy or a cluster of galaxies. This effect was first predicted by Einstein's theory of general relativity in 1915, and it has since been observed and studied by astronomers around the world [51–53]. Gravitational lensing allows us to study objects that are otherwise too distant or faint to observe directly, as the lensing effect can magnify and distort their appearance. Moreover, by analyzing the way in which the light is bent and distorted, we can learn about the properties of the lensing object and the distribution of matter in the universe. Gravitational lensing has, therefore, become an important tool for studying astrophysics and cosmology, providing us with valuable insights into the nature of the universe and the objects within it. For computing gravitational lensing, there are various methods [54]. RIM [55,56] is a particular method used for calculating the bending of light by a black hole. This method is based on the Rindler approximation, which describes the spacetime around a black hole in a simplified way. The RIM also considers the effect of the black hole's rotation on the trajectory of light and calculates the amount of bending that occurs as a result. This method is widely used to study the properties of rotating black holes and has been applied to a variety of problems in astrophysics and cosmology [55,57–67].

In this article, we aim to explore the potential of probing LIV through the gravitational lensing, GFs, and QNMs of RBBHs. Meanwhile, in black hole physics, a GF [68–73] (also known as an absorption coefficient or a transmission coefficient) is the measure of how much of an incoming wave is absorbed by a black hole and how much is scattered or transmitted away. When a wave (such as a photon or a particle) approaches a black hole, it can be partially absorbed by the black hole's gravitational field, and the remaining

energy can be scattered or transmitted away. The probability of absorption depends on the properties of the wave (such as its energy, frequency, and angular momentum) and the properties of the black hole (such as its mass, charge, and spin). A black hole's GF is the ratio of the absorbed flux to the incident flux of the wave. It is called a "greybody" factor because it represents a partial absorption of the wave, as opposed to a complete absorption (which would result in a blackbody spectrum). Namely, GFs are important in black hole physics because they affect the thermal radiation emitted by a black hole (known as Hawking's radiation [74–76]). The Hawking radiation spectrum is related to the GFs of the black hole and can provide information about the properties of the black hole. In summary, GFs are important in the study of black hole thermodynamics and in the search for black hole candidates in astrophysics. In this context, it is one of the important aims of this study to explore the fingerprints of the LIV parameter with GFs with the semi-analytical bound method [71,77–80], which is a powerful technique used in black hole physics to compute the GFs. The semi-analytical bound method (the so-called Miller–Good transformation method [80]) involves combining analytical and numerical techniques to calculate the GFs. The analytical part of the method involves finding a set of bounds on the GFs, based on the properties of the black hole and the radiation being emitted. These bounds can be computed using the perturbation theory. One advantage of the semi-analytical bound method is that it can be applied to a wide range of black hole geometries and radiation types, including scalar, electromagnetic, and gravitational radiation. It is also computationally efficient, making it well-suited for studying the properties of black holes in astrophysical scenarios, such as accretion disks and binary systems [81]. In short, we shall employ the RIM for the gravitational lensing phenomenon, the Miller–Good transformation method for the GF computations, and the unstable circular null geodesic method, whose results are in agreement with the WKB approximation method [82,83], for the derivation of analytical QNMs. As a result, we aim to shed new light on the nature of LIV and its implications for our understanding of the universe. In the meantime, it can be questioned as to why these different subjects are discussed in the same article. We should clarify this issue as follows: Many theories and models have been proposed to explain gravity, each with its own unique features and characteristics. Among the various theories, the bumblebee gravity theory has been studied extensively in recent years. In the bumblebee gravity theory, the vector field responsible for carrying the gravitational force has an additional symmetry that is not present in the GR theory. This symmetry, called gauge symmetry, is a mathematical property that describes the symmetry of the field under certain transformations. One of the important aspects of gravity is its ability to cause gravitational lensing. Gravitational lensing occurs when light passing through a gravitational field is bent, creating a distortion of the image of the object being observed. This effect has been observed in many astronomical phenomena, such as galaxy clusters and black holes. Hence, the bumblebee gravity theory is an interesting area of research in the field of astrophysics. For this reason, it can be studied in conjunction with other important concepts, such as gravitational lensing, GFs, and QNMs, to gain a deeper understanding of the behavior of bumblebee gravity and its interactions with matter. The study of these concepts and their interrelationships have the potential to yield many exciting discoveries about the bumblebee gravity theory in the years to come.

This paper is organized as follows. Section 2 presents a brief review of SRBBH spacetime and its physical features. In Section 3, we study the gravitational lensing of SRBBH and discuss the results obtained by comparing the real astrophysical data of stars. In Section 4, we use the Miller–Good transformation method to compute the GFs of the SRBBH. Then, in Section 5, for a dilatary RBBH spacetime, we derive the analytical QNMs via the unstable circular null geodesic method. Finally, we draw our conclusions in Section 6.

En passant, unless otherwise stated, we use geometrized (natural) units  $G = c = \hbar = k_B = 1$  and  $(-, +, +, +)$  metric signature in this paper.

## 2. RBBH Spacetime

In this section, we will provide a brief overview of the Einstein–bumblebee gravity model and its associated black hole solutions. This model is an example of an extension to the standard general relativity framework. By utilizing the appropriate potential, the bumblebee vector field  $B_\mu$  obtains a non-zero vacuum expectation value, resulting in the breaking of Lorentz symmetry within the gravitational sector. The action for a single bumblebee field  $B_\mu$  that is coupled to gravity can be defined as follows [22,27]

$$S = \int d^4x \sqrt{-g} \left[ \frac{1}{2\kappa} (\mathcal{R} + \varrho B^a B^b \mathcal{R}_{ab}) - \frac{1}{4} (B^{ab} B_{ab} + 4\mathcal{V}) \right] + \mathcal{L}_M, \tag{1}$$

where  $\kappa = 8\pi G_N$ ,  $\mathcal{R}_{ab}$  is the Ricci tensor, and  $\mathcal{R}$  denotes the Ricci scalar. The actual strength of the connection between non-minimal gravity and the bumblebee field is determined by the real coupling constant, which is denoted as  $\varrho$ . The magnitude of the bumblebee field  $B_{ab}$  is specified by a definition of its intensity:

$$B_{ab} = \partial_a B_b - \partial_b B_a. \tag{2}$$

The bumblebee field  $B_a$  has a vacuum expectation value that should not be zero, so a potential  $\mathcal{V}$  is selected accordingly. The potential  $\mathcal{V}$  has a minimum at  $y_0 = B_a B^a \pm b^2$  where  $b$  is a real, positive constant. Therefore, the potential can be represented using the formula given in the 2018 paper by Casana [22].

$$\mathcal{V} = \mathcal{V}(y_0). \tag{3}$$

The possibility of a non-zero vacuum value  $\langle B^a \rangle = b^a$  exists and it can be triggered by a certain potential, which satisfies the condition:  $b_a b^a = \mp b^2$ . The process of calculating the variation in action (1) leads to the formulation of two equations: one describes the behavior of gravity in an empty space (known as the vacuum gravitational equation), and the other describes how the bumblebee field moves (known as the equation of motion for the bumblebee field). Hence, one has

$$\mathcal{R}_{ab} - \frac{1}{2} g_{ab} \mathcal{R} = \kappa T_{ab}^B, \tag{4}$$

$$\nabla^a B_{ab} = 2\mathcal{V}' B_b - \frac{\varrho}{\kappa} B^a \mathcal{R}_{ab}. \tag{5}$$

where  $T_{ab}^B$  denotes the bumblebee energy-momentum tensor [25]:

$$T_{ab}^B = B_{ac} B_a^c - \frac{1}{4} g_{ab} B^{cd} B_{cd} - g_{ab} \mathcal{V} + 2B_a B_b \mathcal{V}' + \frac{\varrho}{\kappa} \left[ \frac{1}{2} g_{ab} B^c B^d \mathcal{R}_{cd} - B_a B^c \mathcal{R}_{cb} - B_b B^c \mathcal{R}_{ca} + \frac{1}{2} \nabla_c \nabla_a (B^c B_b) + \frac{1}{2} \nabla_c \nabla_b (B^c B_a) - \frac{1}{2} \nabla^2 (B_a B_b) - \frac{1}{2} g_{ab} \nabla_c \nabla_d (B^c B^d) \right], \tag{6}$$

Moreover,  $\mathcal{V}' = \partial \mathcal{V}(y) / \partial y$  at  $y = y_0$ . With the trace of Equation (5), one obtains the trace-reversed version:

$$\mathcal{R}_{ab} = \kappa T_{ab}^B + 2\kappa g_{ab} \mathcal{V} - \kappa g_{ab} B^c B_c \mathcal{V}' + \frac{\varrho}{4} g_{ab} (\nabla^2 (B^c B_c) + 2g_{ab} \nabla_c \nabla_d (B^c B^d)). \tag{7}$$

Now, without loss of generality, one can assume that the bumblebee field is frozen at its vacuum expectation value. This assumption makes the specific form of the potential, which is irrelevant to its dynamics, resulting in  $V = 0$  and  $V' = 0$ . With these conditions, the first two terms in Equation (6) are similar to those of the electromagnetic field, except for the coupling terms to the Ricci tensor. Given this, Equation (7) leads to the equations for the gravitational field [25]:  $R_{ab} = 0$ , with

$$R_{ab} = \mathcal{R}_{ab} - \kappa b_{ac} b_b^c + \frac{\kappa}{4} g_{ab} b^{cd} b_{cd} + \varrho b_a b^c \mathcal{R}_{cb} + \varrho b_b b^c \mathcal{R}_{ca} - \frac{\varrho}{2} g_{ab} b^c b^d \mathcal{R}_{cd} + \bar{\mathcal{B}}_{ab}, \tag{8}$$

$$\mathcal{B}_{ab} = -\frac{\rho}{2} \left[ \nabla_c \nabla_a (b^c b_b) + \nabla_c \nabla_b (b^c b_a) - \nabla^2 (b_a b_b) \right]. \tag{9}$$

Overall, the condition of  $R_{ab} = 0$  determines whether the obtained spacetime is an exact solution of the vacuum Einstein–bumblebee action or not. Additional elaborations regarding this matter were presented in a very recent study by Liu et al [49].

In 2020, Ding et al. [25] revealed that by imposing the condition  $b^a b_a = const.$  and utilizing the bumblebee field  $b_a = (0, \rho b_0 \Delta^{1/2}, 0, 0)$ , a Kerr-like black hole solution for the Einstein–bumblebee theory can be obtained. This solution is expressed as follows:

$$ds^2 = -\left(1 - \frac{2Mr}{\rho^2}\right) dt^2 + \rho^2 \left(\frac{1}{\Delta} dr^2 + d\theta^2\right) + \frac{1}{\rho^2} \left(-4Mr\tilde{a} \sin^2 \theta dt d\varphi + \mathcal{A} \sin^2 \theta d\varphi^2\right). \tag{10}$$

where

$$\mathcal{A} = (r^2 + \tilde{a}^2)^2 - \Delta \tilde{a}^2 \sin^2 \theta, \tag{11}$$

$$\rho^2 = r^2 + \tilde{a}^2 \cos^2 \theta, \tag{12}$$

$$\Delta = (1 + \ell)^{-1} (r^2 - 2Mr) + a^2, \tag{13}$$

$$\tilde{a} = \sqrt{1 + \ell} a. \tag{14}$$

The Lorentz-violating parameter (we shall also call it the bumblebee or LSB parameter [84]) in metric (10) is denoted by  $\ell = \rho b_0^2$ , and  $a$  is the rotation parameter; this metric represents a rotating spacetime with a radial bumblebee field. When  $\ell \rightarrow 0$ , the metric reduces to the usual Kerr metric, while it becomes the static Einstein–bumblebee metric when  $a \rightarrow 0$ . However, the metric given in Equation (10) is not a correct RBBH solution according to the findings of Maluf and Muniz [33]; their work was supported by [28,32,49]. In particular, it was shown in [33] that

$$\nabla^\theta b_{\theta r} + \frac{\rho}{\kappa} b^r \mathcal{R}_{rr} \neq 0, \tag{15}$$

$$\nabla^r b_{r\theta} + \frac{\rho}{\kappa} b^r \mathcal{R}_{r\theta} \neq 0. \tag{16}$$

However, it was again emphasized by Maluf and Muniz [33] that metric (10) becomes correct in the slow rotation limit. To address this issue, we can expand the metric to the second order of the rotation parameter  $\tilde{a}$  by assuming that  $\tilde{a}$  is sufficiently small, and we obtain the following metric:

$$ds^2 \approx -\left(1 - \frac{2M}{r} + \frac{2M\tilde{a}^2 \cos^2 \theta}{r^3}\right) dt^2 - \frac{4M\tilde{a} \sin^2 \theta}{r} dt d\varphi + \frac{(1 + \ell)\rho^2}{\tilde{\Delta}} dr^2 + (r^2 + \tilde{a}^2 \cos^2 \theta) d\theta^2 + \sin^2 \theta \left[ r^2 + \tilde{a}^2 \left(1 + \frac{2M}{r} \sin^2 \theta\right) \right] d\varphi^2, \tag{17}$$

In the second order of  $\tilde{a}$ ,  $\tilde{\Delta}$  is the same as  $\Delta$ . This enables us to identify the horizons  $r_+$  (event) and  $r_-$  (inner) by finding the roots of  $\tilde{\Delta}$ .

$$\tilde{\Delta} = (r - r_+)(r - r_-). \tag{18}$$

where

$$r_+ = 2M - r_p, \quad r_- = r_p, \tag{19}$$

in which

$$r_p = \frac{\tilde{a}^2}{2M}. \tag{20}$$

Metric (17) still does not fully satisfy certain components of the field Equation (8). On the other hand, the non-zero terms for the field equations are all linked to the rotation parameter  $a$ . Therefore, metric (17) can be viewed as the *slow* RBBH (SRBBH) estimation of the Einstein–bumblebee equation:  $\bar{R}_{ab} = 0$ . More information about this issue can be found in the Appendix section of Reference [49]. For the slowest or dilatory RBBH (DRBBH), one can consider the case of  $\tilde{a}^2 \rightarrow 0$  and hence  $r_+ \rightarrow 2M$  and  $r_- = r_p \rightarrow 0$ . In this case, metric (17) becomes

$$ds^2 \approx -f(r)dt^2 - \frac{2r_+ \tilde{a} \sin^2 \theta}{r} dt d\varphi + g(r)dr^2 + r^2(d\theta^2 + \sin^2 \theta d\varphi^2), \tag{21}$$

where

$$f(r) = 1 - \frac{r_+}{r}, \tag{22}$$

$$g(r) = \frac{(1 + \ell)}{f(r)}. \tag{23}$$

At this stage, to avoid lengthy computations and prioritize clarity and comprehensibility, let us discuss the thermodynamic features of the DRBBH. To this end, we first consider a particle’s behavior in close proximity to the event horizon by utilizing the following four-velocity [85]:

$$u^\alpha \rightarrow \left( (-g^{tt})^{1/2}, 0, 0, \frac{-g^{t\varphi}}{(-g^{tt})^{1/2}} \right). \tag{24}$$

The zero angular momentum observer (ZAMO) always behaves well because  $g^{tt} < 0$  for all cases outside the horizon ( $r > r_+$ ). The ZAMO always co-rotates with the black hole at the following angular velocity (as seen from spatial infinity):

$$\Omega_{\text{ZAMO}} = \frac{u^\varphi}{u^t} = -\frac{g^{t\varphi}}{g^{tt}} = -\frac{g_{t\varphi}}{g_{\varphi\varphi}} \tag{25}$$

One may ask at a given  $(r, \theta)$  what the range of the allowed  $d\varphi/dt$  is. One can judge that this is possible by the following metric condition:

$$g_{tt} + 2g_{t\varphi} \frac{d\varphi}{dt} + g_{\varphi\varphi} \left( \frac{d\varphi}{dt} \right)^2 < 0, \tag{26}$$

or  $\Omega_{\min} < \frac{d\varphi}{dt} < \Omega_{\max}$  with

$$\Omega_{\max, \min} = \Omega_{\text{ZAMO}} \pm \frac{\sqrt{(g_{t\varphi})^2 - g_{tt}g_{\varphi\varphi}}}{g_{\varphi\varphi}}. \tag{27}$$

What is interesting is that as we approach the event horizon  $r_+$ , although  $g_{\varphi\varphi}$  remains finite,  $\left( (g_{t\varphi})^2 - g_{tt}g_{\varphi\varphi} \right) \rightarrow 0$  ; thus, all particles near the event horizon must have

$$\frac{d\varphi}{dt} \approx \Omega_H = \Omega_{\text{ZAMO}}(r_+) = \frac{a}{r_+^2}. \tag{28}$$

Thus,  $\Omega_H$  is called the angular velocity of the horizon or the black hole. It is obvious that the RBBH metric is stationary and axisymmetric, with Killing fields  $\zeta^a = (\partial/\partial t)^a$  and  $\psi^a = (\partial/\partial \varphi)^a$ . Moreover, the RBBH is asymptotically flat, which can be seen crudely from the fact that the metric components (17) or (21) approach those of the Minkowski spacetime in spherical polar coordinates as  $r \rightarrow \infty$ . Employing the black hole mass definition of Wald [86]

$$\tilde{M} = -\frac{1}{8\pi} \int_S \epsilon_{abcd} \nabla^c \zeta^d, \tag{29}$$

where the integral is taken over a sphere,  $S$ , one can obtain the mass of the DRBBH

$$\tilde{M} = \frac{r_+}{2\sqrt{1+l}} = \frac{M}{\sqrt{1+l}}. \tag{30}$$

Moreover, the total angular momentum of RBBH can be computed via the following expression [86]:

$$J = \frac{1}{16\pi} \int_S \epsilon_{abcd} \nabla^c \psi^d, \tag{31}$$

which yields the following expression for the DRBBH

$$J = \frac{\tilde{a}r_+}{2\sqrt{1+l}} = \frac{ar_+}{2} = Ma. \tag{32}$$

As the metric components solely rely on  $r$  and  $\theta$ , the acceleration of a particle can be derived from

$$a^\alpha = \Gamma_{\mu\nu}^\alpha u^\mu u^\nu = -g^{\alpha\mu} \partial_\mu \ln u^t. \tag{33}$$

According to Reference [86], the surface gravity ( $\kappa$ ) is defined as

$$\kappa = \lim_{r \rightarrow r_+} \sqrt{a^\alpha a_\alpha} (u^t)^{-1}. \tag{34}$$

As an exemplary study, if we apply the above formulation of the surface gravity (i.e., Equation (34)) to metric (21), and make some straightforward calculations, we obtain the surface gravity of the DRBBH as follows

$$\kappa = \frac{1}{2} \partial_r f|_{r=r_+} = \frac{1}{2r_+ \sqrt{1+l}}. \tag{35}$$

Thus, the Hawking temperature of the DRBBH reads

$$T_H = \frac{\kappa}{2\pi} = \frac{1}{4\pi r_+ \sqrt{1+l}}. \tag{36}$$

The black hole area is given by

$$A_{BH} = \int_0^{2\pi} d\varphi \int_0^\pi \sqrt{-g} d\theta = 4\pi r_+^2. \tag{37}$$

Therefore, one can easily derive the entropy of the DRBBH as follows

$$S_{BH} = \frac{A_{BH}}{4\hbar} = \pi r_+^2. \tag{38}$$

The obtained thermodynamical quantities of the DRBBH, which are given in Equations (28), (30), (32), (36), and (38) imply that the first law of thermodynamics [76]

$$\begin{aligned} d\tilde{M} &= T_H dS_{BH} + \Omega_H dJ, \\ &= \frac{dr_+}{2\sqrt{1+l}} + \frac{a^2 dr_+}{2r_+^2}, \end{aligned} \tag{39}$$

holds when  $(\frac{a}{\tilde{M}})^2 \rightarrow 0$ . Thus, both the nearly static DRBBHs and/or the significantly massive DRBBHs satisfy the first law of thermodynamics.

### 3. Gravitational Lensing of SRBBH via RIM

Gravitational lensing is a phenomenon in black hole physics where the intense gravitational field of a black hole bends and distorts the path of light passing near it. This can result in the creation of multiple images of the same source, or even the formation

of a complete ring of light known as the Einstein ring. In the vicinity of a black hole, the strong gravitational field warps spacetime, causing the paths of light rays to curve. This can lead to an effect where a distant object appears distorted or magnified when viewed from a certain angle. This phenomenon is similar to how a magnifying glass bends and focuses light to make objects appear larger. Gravitational lensing has been observed in a variety of astrophysical contexts, including around supermassive black holes at the centers of galaxies, and around smaller black holes in binary systems. In some cases, it has even been used to indirectly detect the presence of black holes themselves, by observing the effects of their gravity on the light from nearby stars or gas. In this section, we shall analyze the gravitational lensing of SRBBH via RIM [56]. This method is based on the invariance of the angle, which is obtained as a result of the scalar product of two vectors:

$$\cos(\psi) = \frac{d^i \delta_i}{\sqrt{(d^i d_i)(\delta^j \delta_j)}} \tag{40}$$

where the vector directions  $d$  and  $\delta$  can be represented geometrically in the standard symmetry plane ( $\theta = \pi/2$  plane), with  $t = const.$ , as shown in Figure 1.

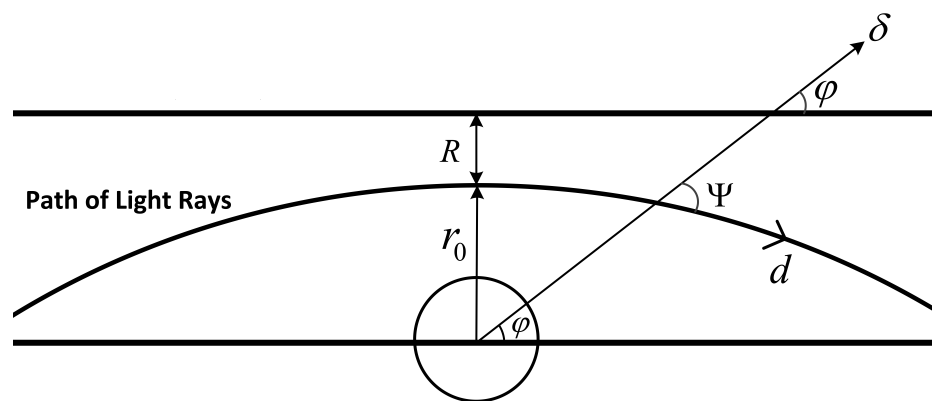


**Figure 1.** The one-sided bending angle is given by  $\epsilon = \psi - \varphi$ . The upper straight line symbolizes the undistorted light rays defined by the solution of the homogeneous part of Equation (45).

The geometrical polar coordinates of the directions can be written as

$$\begin{aligned} d &= (dr, d\varphi) = (A, 1)d\varphi \quad d\varphi < 0, \\ \delta &= (\delta r, 0) = (1, 0)\delta r, \end{aligned} \tag{41}$$

where  $A(r, \varphi) = \frac{dr}{d\varphi}$ . By mapping metric (21) to the following general rotating spacetime:

$$ds^2 = -f(r)dt^2 - 2g(r)dtd\varphi + h(r)dr^2 + p(r)d\varphi^2, \tag{42}$$

in which

$$\begin{aligned} f(r) &= 1 - \frac{2M}{r}, \\ g(r) &= \frac{2M\tilde{a}}{r}, \\ h(r) &= \frac{(\ell + 1)^2}{1 - \frac{2M}{r} + \frac{\tilde{a}^2}{r^2}}, \\ p(r) &= r^2 + \tilde{a}^2 \left(1 - \frac{2M}{r}\right), \end{aligned} \tag{43}$$

One can obtain the following null geodesic equation [87] through the standard change of variable process,  $u = \frac{1}{r}$  (recall the classical Kepler problems), and subsequently derive the evolution of the light curve in the SRBBH spacetime (21):

$$\frac{d^2u}{d\varphi^2} = \frac{1}{2} \frac{d}{du} \left[ \frac{u^4(f(u)p(u) + g^2(u))(p(u) - 2g(u)b - f(u)b^2)}{h^2(u)(g(u) + f(u)b)^2} \right], \tag{44}$$

where  $E$  and  $L$  are the energy and angular momentum of the photon, respectively, and the parameter defined as  $b = E/L$  is called the impact parameter. If we put the metric function into Equation (44), the generic null geodesic equation becomes

$$\frac{d^2u}{d\varphi^2} + \beta u \simeq \frac{Mu^2(-3a^2b(\ell + 1) - 2a\sqrt{\ell + 1}(9a^2(\ell + 1) + 12M^2) + 3b^3)}{b^3(\ell + 1)^2} - \frac{2aM}{b^3(\ell + 1)^{3/2}}, \tag{45}$$

and

$$\beta = \frac{(-3a^2b(\ell + 1) + 8a\sqrt{\ell + 1}M^2 + b^3)^3}{b} (\ell + 1)^2. \tag{46}$$

If we use the standard approximation of  $u = \frac{\sin[\sqrt{\beta}\varphi]}{b}$  to solve Equation (45) and put the homogeneous solution into the inhomogeneous side of Equation (45), then the first order perturbative solution can be found as follows

$$u(\varphi) \approx \frac{\sin[\sqrt{\beta}\varphi]}{b} + \frac{M(\cos(2\sqrt{\beta}\varphi) + 3)}{2b^2\beta(\ell + 1)^2} - \frac{2aM}{b^3\beta(\ell + 1)^{3/2}} + O\left(\frac{1}{b}\right)^4. \tag{47}$$

The closed distance approach  $r_0$  is analyzed at  $\varphi = \pi/2$ . Thus, one can obtain the closed distance as follows

$$\frac{1}{r_0} = \frac{\sin[\sqrt{\beta}\pi/2]}{b} + \frac{M(\cos(\sqrt{\beta}\pi) + 3)}{2b^2\beta(\ell + 1)^2} - \frac{2aM}{b^3\beta(\ell + 1)^{3/2}}. \tag{48}$$

The invariant formula of RIM for the rotating spacetimes is given by [87]

$$\tan(\Psi) = \frac{[h^{-1}(r)p(r)]^{1/2}}{|A(r, \varphi)|}. \tag{49}$$

When we substitute Equation (47) into the definition of  $A(r, \varphi)$ , we can find

$$A(r, \varphi) = -\frac{(\cos(\sqrt{\beta}\varphi)(b\beta(\ell + 1)^2 - 2M\sin(\sqrt{\beta}\varphi))}{b^2\sqrt{\beta}(\ell + 1)^2} r^2. \tag{50}$$

If we use the standard approximations of the RIM,  $\varphi = 0$  and  $\frac{M}{R} \ll 1$ , Equations (47) and (50) then yield

$$r \approx \frac{b^2\beta(\ell + 1)^2}{2M}, \quad A(r, \varphi = 0) \approx -r^2 \frac{\sqrt{\beta}}{b}. \tag{51}$$

When we use expression (51) and the related metric functions, Equation (43) in Equation (49), and perform the small angle approximation,  $\epsilon = \tan\psi_0 \approx \psi_0$ , the bending angle of the SRBBH can be found as follows:

$$\epsilon \approx \frac{2M}{\beta^{3/2}(\ell + 1)^3 b} \left\{ 1 - \frac{2M^2}{\beta(1 + \ell)^2 b^2} + \frac{4M^2 a^2}{\beta^2(1 + \ell)^3 b^4} - \frac{16M^4 a^2}{\beta^3(1 + \ell)^5 b^6} + \frac{8M^2(a^4(\ell + 1)M^2 + 4a^2M^4)}{\beta^4(\ell + 1)^7 b^8} \right\} + O\left(\frac{1}{b}\right)^9. \tag{52}$$

We analyzed the gravitational lensing phenomenon for stars whose masses, radii, and rotational parameters are recorded in Reference [87], for specific values of the  $\ell$  parameter, by utilizing the graphs presented in Figure 2. The analysis of the plots depicted in Figure 2 for various real stars observed in the cosmos demonstrates a clear correlation between the bumblebee parameter  $\ell$  and the bending angle at low  $\frac{b}{R_{star}}$  values. It is worth noting that the units used in the calculation are first converted to standard international units, or S.I units. In order to convert the mass ( $M$ ) to S.I units, it is multiplied by  $Gc^{-2}$ , where  $G = 6.67408 \times 10^{-11} \text{ m}^3\text{kg}^{-1}\text{s}^{-2}$  is the gravitational constant and  $c = 3 \times 10^8 \text{ ms}^{-1}$  is the speed of light. This results in the one-sided bending angle being measured in radians. Specifically, as the value of  $\ell$  increases, the bending angle also increases. This observation suggests that the bumblebee parameter plays a crucial role in determining the gravitational lensing effects of stars. Furthermore, this trend is only observed at low  $\frac{b}{R_{star}}$  values, which indicates that the impact of the bumblebee parameter may be negligible under certain conditions. Overall, these findings provide valuable insights into the underlying physics of gravitational lensing and offer a potential avenue for further investigation into the nature of the bumblebee parameter and its role in gravitational lensing.

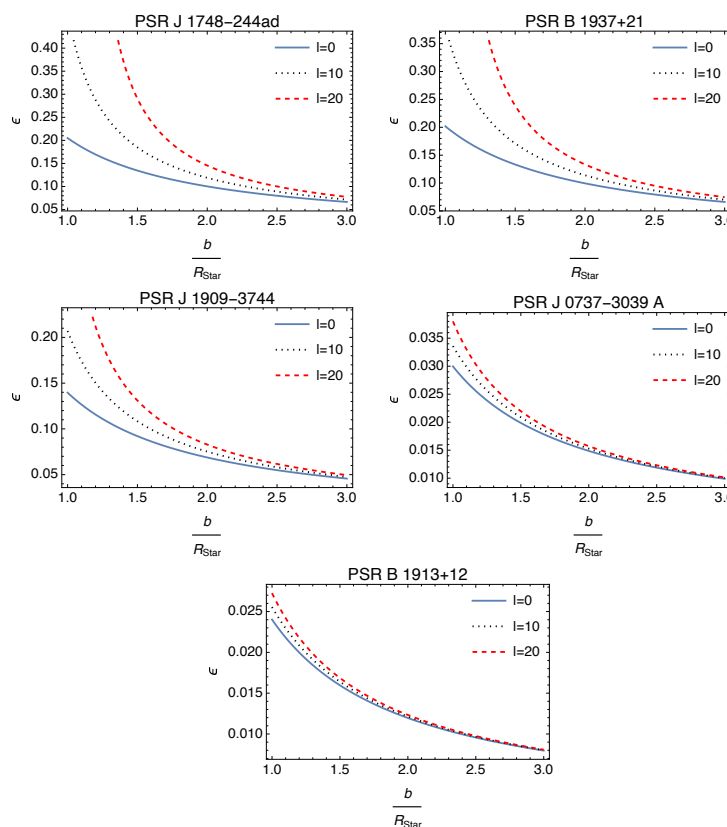


**Figure 2.** Bending angle  $\epsilon$  versus  $\frac{b}{R_{star}}$  graphs. The  $R_{star}$  represents the radius of the star entitled in each graph. The effects of varying bumblebee parameters on the bending angle are illustrated.

#### 4. GFs of SRBBH Spacetime

The calculation of GFs is an important aspect of studying black hole thermodynamics and Hawking’s radiation. According to Hawking’s famous calculation [74,75], black holes emit radiation due to quantum effects, and radiation has a thermal spectrum with a

temperature proportional to the black hole’s surface gravity. However, this calculation assumes that the black hole is a blackbody, namely a perfect absorber, which is not the case in reality. The GF takes into account the deviation from perfect absorption and modifies the thermal spectrum accordingly. In this section, our aim is to derive the GFs of the SRBBH spacetime. In this regard, we use the massive Klein–Gordon equation, which plays an important role in the study of black hole physics. It is a relativistic wave equation that describes the behavior of a scalar field in the presence of a massive particle. In the context of black holes, this equation is often used to describe the behavior of matter fields around black holes. In general, the massive Klein–Gordon equation can be written as [6]:

$$\frac{1}{\sqrt{-g}}\partial_\mu(\sqrt{-g}g^{\mu\nu}\partial_\nu\phi) = \mu^2\phi, \tag{53}$$

where  $\mu$  indicates the mass of the scalar field. By substituting metric (21) in Equation (53) with the following ansatz:

$$\phi = \frac{\Psi(r)}{\sqrt{r^2 + a^2}}e^{-i\omega t}Y(\theta, \phi), \tag{54}$$

and, in the sequel, expanding the result up to the first order of  $\tilde{a}$ , we have as follows (for a similar analysis, the reader is referred to [49] and references therein):

$$\frac{d^2}{dx^2}\Psi_l^{(1)} + V_l^{(1)}\Psi_l^{(1)} = 0, \tag{55}$$

where  $dr/dx = F = 1 - \frac{2M}{r}$ . The effective potential  $V_l^{(1)}$  is given by

$$V_l^{(1)} = (1 + \ell)\left(\omega^2 - \sqrt{1 + \ell}\frac{4amM\omega}{r^3}\right) - F\left(\frac{2M}{r^3} + (1 + \ell)\left(\frac{\lambda}{r^2} + \mu^2\right)\right). \tag{56}$$

In Equation (56),  $\lambda = l(l + 1)$  is the eigenvalue of the wave equation and  $l$  stands for the angular quantum number. Moreover, the second-order expansion of Equation (53) with respect to  $\tilde{a}$  recasts in

$$\frac{d^2}{dr_*^2}Z_l + V_l^{(2)}Z_l = 0, \tag{57}$$

where  $\frac{dr}{dr_*} = \frac{(1+\ell)\delta}{r^2+a^2}$  and

$$Z_l = \Psi_l^{(2)} + a^2c_l\Psi_{l-2}^{(2)} - a^2c_{l+2}\Psi_{l+2}^{(2)}, \tag{58}$$

in which

$$c_l = \frac{(1 + l)(\mu^2 - \omega^2)}{2(2l - 1)}\sqrt{\frac{(l - 1)^2 - m^2}{4(l - 1)^2 - 1}}\sqrt{\frac{l^2 - m^2}{4l^2 - 1}}. \tag{59}$$

Furthermore, the effective potential in Equation (57) can be found as follows

$$\begin{aligned} V_l^{(2)} = & V_l^{(1)} - \frac{24M^2a^2}{r^6} + \frac{2Ma^2}{r^5}(6 - 2l(l + 1)(1 + \ell) - 3\ell - 2r^2(1 + \ell)\mu^2 + r^2(1 + \ell)^2\omega^2) \\ & + \frac{a^2}{r^4}(l - 1 + 2\ell - l\ell^2 + m^2(1 + \ell)^2 - l^2(\ell^2 - 1) + r^2\mu^2 - r^2(\omega^2 + \ell^2\mu^2 - \ell^2\omega^2)) \\ & - \frac{a^2F}{r^2}(1 + \ell)^2(\mu^2 - \omega^2)\left(\frac{l^2 - m^2}{4l^2 - 1}\right)\left(\frac{(l + 1)^2 - m^2}{4(l + 1)^2 - 1}\right). \end{aligned} \tag{60}$$

Figure 3 shows the effective potentials represented in Equations (56) and (60). It is evident that the effective potentials increase as a barrier with the increase of the bumblebee parameter  $\ell$ .

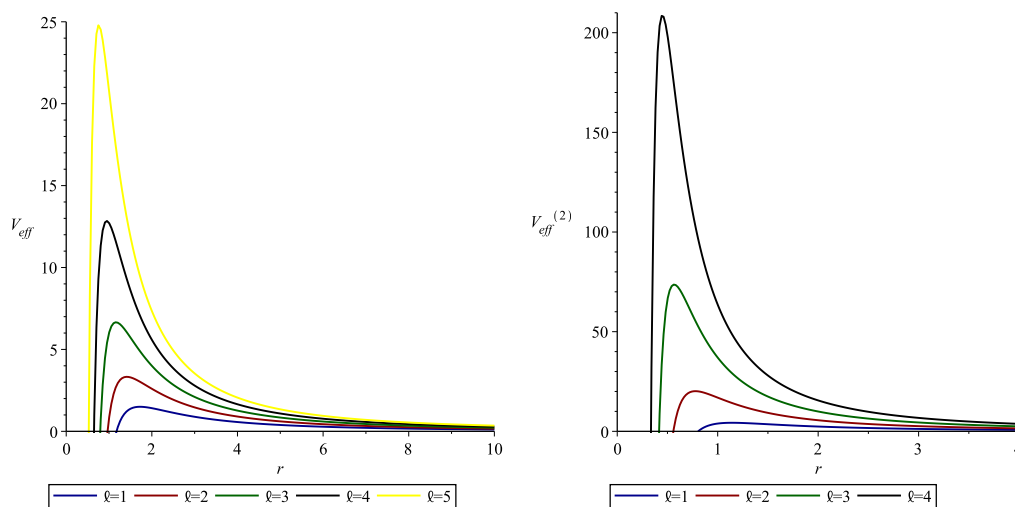


**Figure 3.**  $\sigma_l(\omega)$  versus  $\omega$  graphs of the effective potential for the first order (**left**) and second order (**right**) of  $\tilde{a}$ . The physical parameters are chosen as  $M = m = 1, \tilde{a} = 0.1, \lambda = 6 (l = 2)$ , and  $\omega = 10$ .

To derive the GFs, we apply the general semi-analytic bounds, defined by

$$\sigma(\omega) \geq \sec h^2 \left[ \int_{-\infty}^{+\infty} \wp dr_* \right], \tag{61}$$

where

$$\wp = \frac{\sqrt{(h'^2) + (\omega^2 - V_{eff} - h^2)^2}}{2h}, \tag{62}$$

In which  $h(x)$ , seen in the integrand of Equation (61), is a positive function that fulfills the two conditions: (1)  $h(r_*) > 0$  and (2)  $h(-\infty) = h(+\infty) = \omega$ . After applying the aforementioned conditions to the effective potentials, one may observe a direct proportionality between the GFs and the effective potential, where the metric function plays a significant action in this process. Thus, Equation (61) becomes

$$\sigma(\omega) \geq \sec h^2 \left[ \int_{r_h}^{+\infty} \frac{V_{eff}}{2\omega} \frac{dr}{dr_*} \right]. \tag{63}$$

One advantage of using a massless scalar field is that it allows for the propagation of waves at the speed of light, which is a fundamental feature of many physical systems. Additionally, massless fields are mathematically simpler to work with and can lead to more elegant and concise solutions to certain problems. For this reason, by taking cognizance of massless fields and substituting Equation (56) in Equation (63) with  $\frac{dr}{dr_*} \equiv \frac{dr}{dx}$ , one can obtain the GFs of the SRBBH for the first order of  $\tilde{a}$  as follows

$$\sigma_\ell^{(1)}(\omega) \geq \sec h^2 \left( \frac{1}{2\omega} \left[ 4aMm\omega((1 + \ell)\sqrt{1 + \ell}) \left( \frac{1}{2r_h^2} + \frac{2M}{3r_h^3} + \frac{M^2}{r_h^4} + \frac{8M^3}{5r_h^5} \right) + \frac{M + r_h\lambda(1 + \ell)}{r_h^2} \right] \right). \tag{64}$$

The behavior of the GFs for the first order of the rotating parameter  $\tilde{a}$  for the varying bumblebee parameter  $\ell$  is depicted in Figure 4. The figure demonstrates that increasing the bumblebee parameter  $\ell$  results in a decreased probability of encountering Hawking radiations.

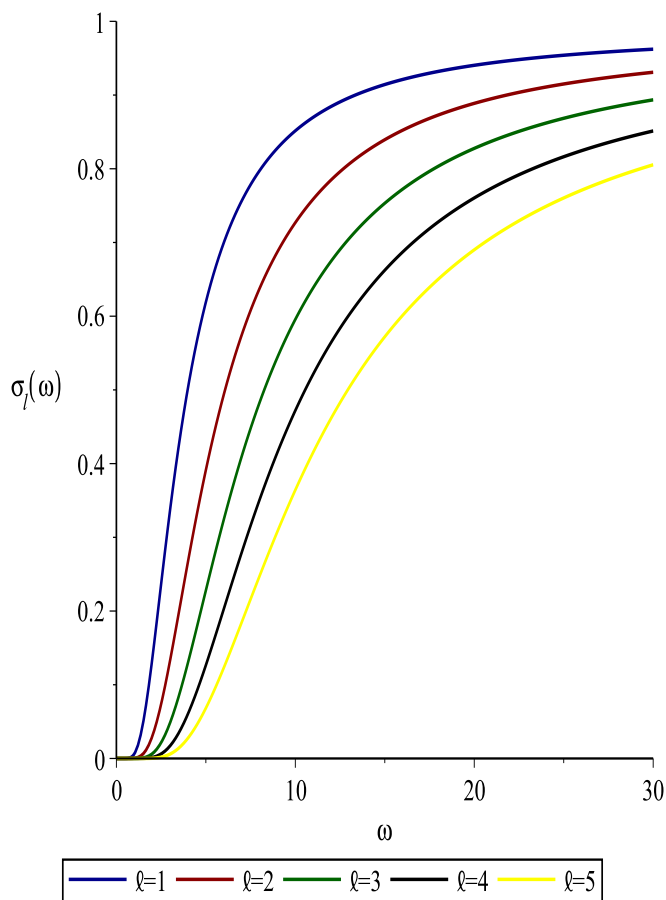


**Figure 4.**  $\sigma_l(\omega)$  versus  $\omega$  graphs for the massless scalar field propagating in the SRBBH with the first-order expansion of  $\tilde{a}$ . The physical parameters are chosen as  $M = 1, \lambda = 6$ , and  $\tilde{a} = 0.1$

The GFs for the second order of  $\tilde{a}$  can be determined using a similar procedure by substituting Equation (60) into Equation (63). One can obtain

$$\sigma_\ell(\omega)^{(2)} \geq \left[ \sigma_\ell^{(1)}(\omega) + \sec h^2 \left( \frac{1}{2\omega(1+\ell)} \left[ \frac{-A}{7r_h^7} + \frac{B}{6r_h^6} + \frac{C}{5r_h^5} + \frac{D}{4r_h^4} + \frac{E}{3r_h^3} + \frac{H}{2r_h^2} \right] \right) \right], \tag{65}$$

by which

$$A = 24M^2a^2(a^2 - r_+r_- + 4M^2), \tag{66}$$

$$B = 2Ma^2(a^2 - r_+r_- + 4M^2)(6 - 2l(l+1)(1+\ell) + 3\ell) - 48M^3a^2, \tag{67}$$

$$C = a^2(a^2 - r_+r_- + 4M^2)(l - 1 + 2\ell - \ell^2l + m^2(1+\ell)^2 - l^2(\ell^2 - 1)) + 4M^2a^2(3\ell - 2l(l+1)(1+\ell)), \tag{68}$$

$$D = 2Ma^2(1+\ell)^2\omega^2(a^2 - r_+r_- + 4M^2) + 2Ma^2(l - 1 + 2\ell - l\ell^2 + m^2(1+\ell)^2 - l^2(\ell^2 - 1)) + 2Ma^2(6 - 2l(l+1)(1+\ell) + 3\ell), \tag{69}$$

$$E = Fa^2(1+\ell)^2\omega^2(a^2 - r_+r_- + 4M^2) \left( \frac{l^2 - m^2}{4l^2 - 1} + \frac{(l+1)^2 - m^2}{4(l+1)^2 - 1} \right) - a^2\omega^2(a^2 - r_+r_- + 4M^2) \times (1 + \ell^2) + 4M^2a^2(1+\ell)^2\omega^2 + a^2(l - 1 + 2\ell - l\ell^2 + m^2(1+\ell)^2 - l^2(\ell^2 - 1)), \tag{70}$$

$$H = 2Ma^2(1 + \ell)^2\omega^2 - 2Ma^2\omega^2(1 + \ell^2) + 2FMa^2(1 + \ell)^2\omega^2\left(\frac{l^2 - m^2}{4l^2 - 1} + \frac{(l + 1)^2 - m^2}{4(l + 1)^2 - 1}\right), \tag{71}$$

where  $r_+r_- = (2M - (1 + \ell)\frac{a^2}{2M})(1 + \ell)\frac{a^2}{2M}$ . Figure 5 represents the relationship between the GFs of the second order of  $\tilde{a}$  and the bumblebee parameters. The right figure is drawn for both the first order  $\sigma_\ell(\omega)$  and second order  $\sigma_\ell^{(2)}(\omega)$ ; however, the left figure represents the GFs of the SRBBH together with the first and second orders of  $\sigma_\ell(\omega)$ , i.e., Equation (65). Again, it is obvious that the increase in the  $\ell$  parameter decreases the GFs.

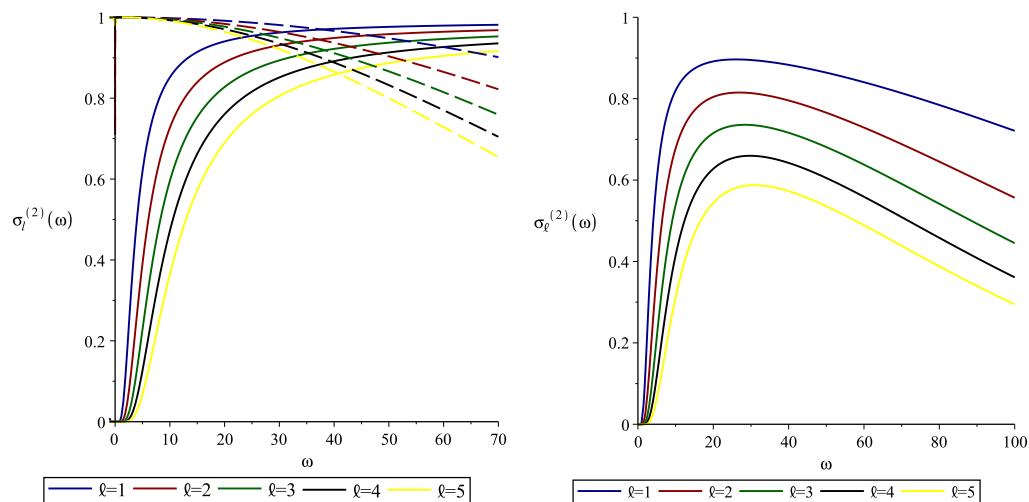


**Figure 5.**  $\sigma_l(\omega)$  versus the  $\omega$  graph for the massless scalar field and first-order expansion of  $\tilde{a}$  for RBBH. The left figure represents the GFs of SRBBH for both the first order (solid lines) and second order (dashed line) of  $\tilde{a}$ . The right one shows the GFs of the SRBBH with the combination of both the first and second orders of  $\tilde{a}$ ; see Equation (65).

### 5. QNMs of Extremely Slow Rotating DRBBH via Unstable Circular Null Geodesic Method

Ever since the unveiling of the LIGO experiment [88], there has been an increased interest in gravitational waves, specifically those emitted by disturbed black holes. These waves are predominantly characterized by “quasinormal ringing” [89], which refers to the damped oscillations at specific frequencies that are unique to the system in question. These QNM frequencies can be determined by calculating the scalar perturbation of a massless field around a black hole:

$$\partial_\mu(\sqrt{-g}g^{\mu\nu}\partial_\nu\Psi) = 0. \tag{72}$$

In the extreme slow-rotation approximation, the DRBBH metric (21) can be approximated to the static bumblebee black hole [22], which is given by

$$ds^2 \approx -F(r)dt^2 + \frac{1}{g(r)}dr^2 + r^2(d\theta^2 + \sin^2\theta d\varphi^2), \tag{73}$$

where we recall that  $F(r) = 1 - \frac{2M}{r}$  and

$$g(r) = (\ell + 1)\left(1 - \frac{2M}{r}\right). \tag{74}$$

One can separate the scalar wave Equation (72) by considering the following ansatz:

$$\Psi = R(r)Y_{lm}(\vartheta)e^{im\phi}e^{-i\omega t}, \tag{75}$$

where  $R(r)$  is nothing but the radial function and  $Y_{lm}$  denotes the spherical harmonics. By employing the tortoise coordinate transformation  $r_* = \int \frac{dr}{\sqrt{f(r)g(r)}}$ , Equation (72) reduces to a one-dimensional Schrödinger-like wave equation:

$$\frac{d^2R(r_*)}{dr_*^2} + (\omega^2 - V(r_*))R(r_*) = 0, \tag{76}$$

where  $\omega = \omega_R - i\omega_I$  is a complex quasinormal mode frequency and the effective potential read is given by [90]

$$V(r) = H(r) \left( \frac{H'(r)}{r} - \frac{l(l+1)}{r^2} \right), \tag{77}$$

where  $H(r) = \sqrt{f(r)g(r)}$ ; recall that  $l$  is the angular quantum number, and the prime symbol denotes the derivative with respect to  $r$ . Hence, one obtains

$$V(r) = \frac{(r - 2M) \left( \frac{2M}{r^3\sqrt{1+l}} + \frac{l(l+1)}{r^2} \right)}{r\sqrt{1+l}}. \tag{78}$$

The behaviors of the effective potential for the massless bosonic waves propagating in the extremely slow-spinning DRBBH geometry (73) are depicted in Figure 6. It is clear from the figure that increasing the bumblebee parameter  $\ell$  decreases the height of the potential barrier, while increasing the angular quantum number  $l$  increases the apex of the barrier.

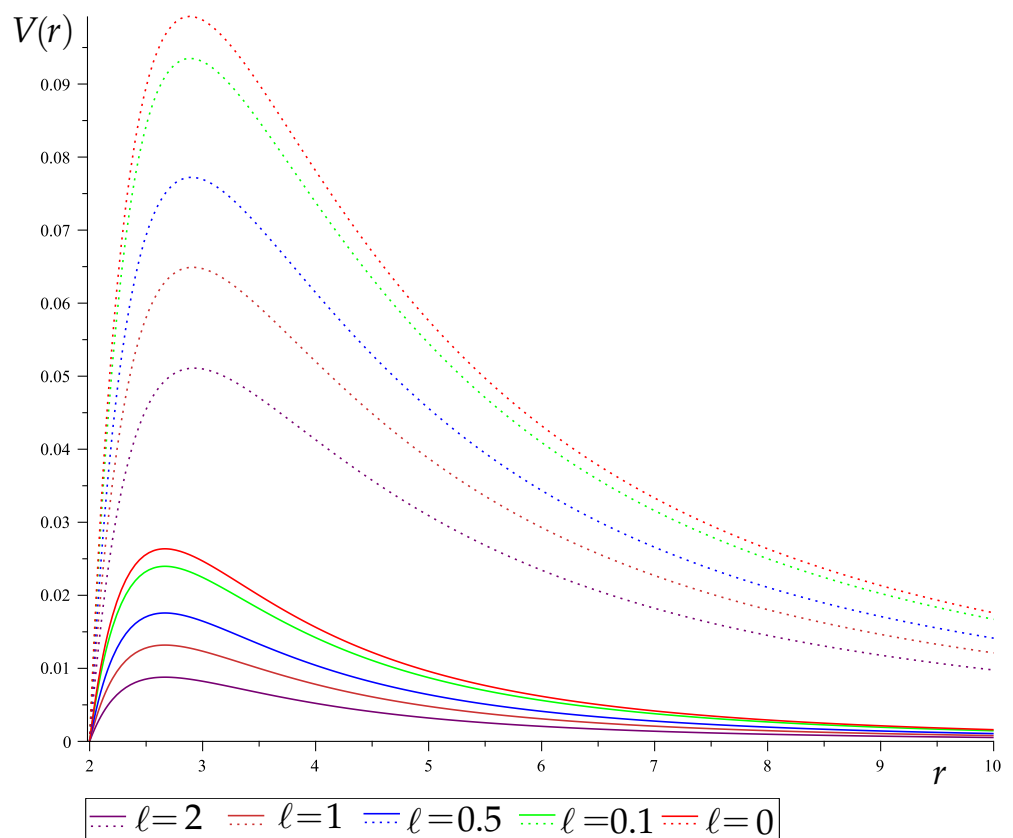


**Figure 6.** Plots of effective potential (78) for massless spin-0 waves propagating in the extremely slow-spinning DRBBH (73). The physical parameters are chosen as  $M = 1$  and  $a \approx 0$ . The curves are labeled by the values of  $l$ :  $l = 0$  curves are represented by solid lines; dotted curves stand for  $l = 1$ .

In Reference [82], it was noted that the parameters governing the unstable circular null geodesics around any stationary spherically symmetric and asymptotically flat black holes—such as the angular velocity  $\Omega_C$  and the principal Lyapunov exponent  $\lambda_{\text{Lexp}}$ —have a remarkable correspondence with the QNMs emitted by the black hole in the eikonal (i.e., short wavelengths or high  $l$  number) part of its spectrum, as discussed in Reference [7]. We now employ the WKB approximation method [91] along with the unstable circular null geodesic method [92] to determine the frequency of the quasinormal mode. Specifically, in the large- $l$  limit, it was shown that the eikonal QNM frequencies are given by [82]

$$\omega_{l \gg 1} = l\Omega_C - \frac{i}{2}(2n + 1)|\lambda_{\text{Lexp}}|, \tag{79}$$

where  $n = 0, 1, 2, \dots$  is the overtone number,  $\lambda_{\text{Lexp}}$  denotes the Lyapunov exponent, and  $\Omega_C$  represents the angular velocity at the unstable null geodesics, which is given by [83,93]

$$\Omega_C = \frac{\sqrt{H(r_{ps})}}{r_{ps}}, \tag{80}$$

where  $r_{ps}$  is the radius of the photon sphere, which can be calculated by finding the largest root of this relation:

$$\frac{H(r_{ps})}{H'(r_{ps})} = \frac{-2Mr_{ps} + r_{ps}^2}{2M} = \frac{r_{ps}}{2}. \tag{81}$$

After making a straightforward calculation, one can easily find that  $r_{ps} = 3M$ . The expression of  $\lambda_{\text{Lexp}}$  can be derived as follows [82]

$$\lambda_{\text{Lexp}} = \sqrt{H(r_{ps}) \left[ \frac{H(r_{ps})}{r_{ps}^2} - \frac{1}{2}H''(r_{ps}) \right]}. \tag{82}$$

Table 1 illustrates the behaviors of the QNMs under varying values of the bumblebee parameter  $\ell$ , angular quantum number  $l$ , and overtone number  $n$ . Specifically, we observe that as  $\ell$  increases, both the real and imaginary parts of the QNMs change. The real part ( $Re(\omega)$ ) corresponds to the frequency of oscillations, while the imaginary part ( $Im(\omega)$ ) dictates the rate at which the oscillations decay. Interestingly, all of the QNMs shown in Table 1 have negative imaginary parts, indicating that they are stable modes. In short, increasing the value of  $\ell$  results in a decrease in the frequency  $\omega$  of the scalar perturbations, which in turn causes the oscillations to decay more slowly. In other words, the higher values of  $\ell$  correspond to longer-lived oscillations. Moreover, one can also observe that the increments in the  $l$  and  $n$ -values increase the values of  $Re(\omega)$  and  $Im(\omega)$ , respectively.

**Table 1.** Effects of the bumblebee parameter  $\ell$ , angular quantum number  $l$ , and the overtone number  $n$  on the QNM frequencies for the fixed mass parameter  $M = 1$ .

$\ell$	$l$	$n$	$Re(\omega)$	$Im(\omega)$
0	0	0	0	−0.09622504490
0	0	1	0	−0.2886751347
0	0	2	0	−0.4811252245
0	1	0	0.1924500898	−0.09622504490
0	1	1	0.1924500898	−0.2886751347
0	1	2	0.1924500898	−0.4811252245
0	2	0	0.3849001795	−0.09622504490
0	2	1	0.3849001795	−0.2886751347
0	2	2	0.3849001795	−0.4811252245
0.1	0	0	0	−0.09174698047
0.1	0	1	0	−0.2752409415

**Table 1.** *Cont.*

$\ell$	$l$	$n$	$Re(\omega)$	$Im(\omega)$
0.1	0	2	0	−0.4587349024
0.1	1	0	0.1879186773	−0.09174698047
0.1	1	1	0.1879186773	−0.2752409415
0.1	1	2	0.1879186773	−0.4587349024
0.1	2	0	0.3758373544	−0.09174698047
0.1	2	1	0.3758373544	−0.2752409415
0.1	2	2	0.3758373544	−0.4587349024
1	0	0	0	−0.06804138176
1	0	1	0	−0.2041241452
1	0	2	0	−0.3402069088
1	1	0	0.1618305907	−0.06804138176
1	1	1	0.1618305907	−0.2041241452
1	1	2	0.1618305907	−0.3402069088
1	2	0	0.3236611813	−0.06804138176
1	2	1	0.3236611813	−0.2041241452
1	2	2	0.3236611813	−0.3402069088

**6. Conclusions**

In this paper, we presented a comprehensive discussion on gravitational lensing, GFs, and QNMs in RBBH spacetime. The study has provided impressive results in four dimensions when considering general relativity coupled with the bumblebee theory. After introducing some physical features of the SRBBH, which was proven to be the more physically correct metric version of RBBH (17), to compute the gravitational lensing, we employed the RIM. The null geodesics and spherical photon orbit conditions were discussed to describe the gravitational lensing of SRBBH. By adjusting the Lorentz-violating parameter  $\ell$  and modeling real stars to the SRBBH spacetime, gravitational lensing was depicted and its usual behavior was explored. We found that the presence of the Lorentz-violating parameter  $\ell$  affects the bending angle of light moving in the SRBBH geometry, which increases with an increase in the Lorentz-violating parameter  $\ell$ . In summary, this result provides compelling evidence for indirectly detecting the existence of the Lorentz-violating parameter  $\ell$  and is, thus, a confirmation of the bumblebee gravity theory.

In a further analysis, we discussed the scattering by using massive bosonic fields via the Klein–Gordon equation in SRBBH. In the sequel, we computed the GFs of the SRBBH by applying the semi-analytical bounds method. It has been found that the GFs of the SRBBH decrease with the increasing Lorentz-violating parameter  $\ell$ . We then extended our analysis to determine the QNM frequencies of the DRBBH. To this end, the null geodesics and spherical photon orbit conditions were discussed in order to employ the unstable circular null geodesic method using the Lyapunov exponents. After obtaining the one-dimensional Schrödinger-like wave equation from the radial part of the Klein–Gordon equation, we illustrated the obtained effective potentials in Figure 6 by varying the bumblebee parameter  $\ell$ , overtone number  $n$ , and angular quantum number  $l$ . We found that the existence of the Lorentz-violating parameter  $\ell$  affects the potential barrier in such a manner that the peak values of the potentials reduce with the increasing bumblebee parameter  $\ell$ . Finally, we explored the QNMs in the large  $l$ -limit, which consists of the imaginary (decaying) and real (oscillatory) parts. Our results show that both oscillatory and decaying sectors of the QNMs decrease with an increase in the magnitude of the Lorentz-violating parameter  $\ell$ .

Our work can be extended to Kerr-like RBBH spacetimes for polarized light [27] as it opens up a new avenue to understand the bumblebee vector field with LSB and its interaction with the electromagnetic fields. Hence, the study of gravitational lensing, GFs, and QNMs in the effective bumblebee gravity metric for polarized light will be a natural extension of our work in the near future. Another possible future problem of bumblebee gravity in black hole physics is that it could lead to the formation of exotic objects known as “gravastars” [94]. These objects are believed to be made up of a type of dark energy

that can counteract the effects of gravity and prevent the formation of a singularity at the center of a black hole. While gravastars are still hypothetical, they could have important implications for our understanding of black hole physics and the nature of dark energy. We will also keep this issue among our possible future works.

**Author Contributions:** Conceptualization, İ.S. and M.M.; methodology, M.M. and S.K.; software, M.M. and S.K.; validation, İ.S., H.G., M.M. and S.K.; formal analysis, İ.S.; investigation, H.G. and İ.S.; resources, İ.S.; data curation, S.K.; writing—original draft preparation, İ.S., M.M. and S.K.; writing—review and editing, H.G.; visualization, S.K. and M.M.; supervision, İ.S.; project administration, İ.S. All authors have read and agreed to the published version of the manuscript.

**Funding:** This research received no external funding.

**Data Availability Statement:** Data sharing not applicable.

**Acknowledgments:** We would like to express our gratitude to the editor and anonymous referees for their valuable suggestions and comments. İ.S. and S.K. would like to acknowledge networking support of COST Action CA18108—Quantum gravity phenomenology in the multi-messenger approach. We also thank TÜBİTAK and SCOAP3 for their support.

**Conflicts of Interest:** The authors declare no conflict of interest.

## References

1. Wiesendanger, C. Local Lorentz invariance and a new theory of gravitation equivalent to General Relativity. *Class. Quant. Grav.* **2018**, *36*, 065015. [[CrossRef](#)]
2. Bailey, Q.G.; Kostelecky, V.A. Signals for Lorentz violation in post-Newtonian gravity. *Phys. Rev. D* **2006**, *74*, 045001. [[CrossRef](#)]
3. Greenberg, O.W. CPT violation implies violation of Lorentz invariance. *Phys. Rev. Lett.* **2002**, *89*, 231602. [[CrossRef](#)]
4. Betschart, G.; Kant, E.; Klinkhamer, F.R. Lorentz violation and black-hole thermodynamics. *Nucl. Phys. B* **2009**, *815*, 198–214. [[CrossRef](#)]
5. Khodadi, M. Black Hole Superradiance in the Presence of Lorentz Symmetry Violation. *Phys. Rev. D* **2021**, *103*, 064051. [[CrossRef](#)]
6. Kanzi, S.; Sakalli, İ. GUP Modified Hawking Radiation in Bumblebee Gravity. *Nucl. Phys. B* **2019**, *946*, 114703. [[CrossRef](#)]
7. Khlebnikov, S. Bulk black hole, escaping photons, and bounds on violations of Lorentz invariance. *Phys. Rev. D* **2007**, *75*, 065021. [[CrossRef](#)]
8. Feng, Z.W.; Ding, Q.C.; Yang, S.Z. Modified fermion tunneling from higher-dimensional charged AdS black hole in massive gravity. *Eur. Phys. J. C* **2019**, *79*, 445. [[CrossRef](#)]
9. Feng, Z.W.; Li, H.L.; Zu, X.T.; Yang, S.Z. Corrections to the thermodynamics of Schwarzschild-Tangherlini black hole and the generalized uncertainty principle. *Eur. Phys. J. C* **2016**, *76*, 212. [[CrossRef](#)]
10. Khodadi, M.; Lambiase, G. Probing Lorentz symmetry violation using the first image of Sagittarius A\*: Constraints on standard-model extension coefficients. *Phys. Rev. D* **2022**, *106*, 104050. [[CrossRef](#)]
11. Neves, J.C.S. Kasner cosmology in bumblebee gravity. *arXiv* **2022**, arXiv:2209.00589.
12. Delhom, A.; Nascimento, J.R.; Olmo, G.J.; Petrov, A.Y.; Porfirio, P.J. Metric-affine bumblebee gravity: Classical aspects. *Eur. Phys. J. C* **2021**, *81*, 287. [[CrossRef](#)]
13. Halprin, A.; Kim, H.B. Mapping Lorentz invariance violations into equivalence principle violations. *Phys. Lett. B* **1999**, *469*, 78–80. [[CrossRef](#)]
14. Lehnert, R. CPT and Lorentz-invariance violation. *Hyperfine Interact. Hyperfine Interact.* **2009**, *193*, 275–281. [[CrossRef](#)]
15. Torri, M.D.C. Neutrino Oscillations and Lorentz Invariance Violation. *Universe* **2020**, *6*, 37. [[CrossRef](#)]
16. Tanabashi, M.; Hagiwara, K.; Hikasa, K.; Nakamura, K.; Sumino, Y.; Takahashi, F.; Tanaka, J.; Agashe, K.; Aielli, G.; Amsler, C.; et al. Review of Particle Physics: Particle data groups. *J. Phys. G* **2006**, *33*, 1–1232.
17. Chan, H.M.; Tsou, S.T. A Model Behind the Standard Model. *Eur. Phys. J. C* **2007**, *52*, 635–663. [[CrossRef](#)]
18. Kostelecky, A.V.; Tasson, J.D. Matter-gravity couplings and Lorentz violation. *Phys. Rev. D* **2011**, *83*, 016013. [[CrossRef](#)]
19. Bluhm, R.; Kostelecky, V.A. Spontaneous Lorentz violation, Nambu-Goldstone modes, and gravity. *Phys. Rev. D* **2005**, *71*, 065008. [[CrossRef](#)]
20. Bluhm, R.; Fun, S.H.; Kostelecky, V.A. Spontaneous Lorentz and Diffeomorphism Violation, Massive Modes, and Gravity. *Phys. Rev. D* **2008**, *77*, 065020. [[CrossRef](#)]
21. Bertolami, O.; Paramos, J. The Flight of the bumblebee: Vacuum solutions of a gravity model with vector-induced spontaneous Lorentz symmetry breaking. *Phys. Rev. D* **2005**, *72*, 044001. [[CrossRef](#)]
22. Casana, R.; Cavalcante, A.; Poulis, F.P.; Santos, E.B. Exact Schwarzschild-like solution in a bumblebee gravity model. *Phys. Rev. D* **2018**, *97*, 104001. [[CrossRef](#)]
23. Li, Z.; Övgün, A. Finite-distance gravitational deflection of massive particles by a Kerr-like black hole in the bumblebee gravity model. *Phys. Rev. D* **2020**, *101*, 024040. [[CrossRef](#)]

24. Li, Z.; Zhang, G.; Övgün, A. Circular Orbit of a Particle and Weak Gravitational Lensing. *Phys. Rev. D* **2020**, *101*, 124058. [[CrossRef](#)]
25. Ding, C.; Liu, C.; Casana, R.; Cavalcante, A. Exact Kerr-like solution and its shadow in a gravity model with spontaneous Lorentz symmetry breaking. *Eur. Phys. J. C* **2020**, *80*, 178. [[CrossRef](#)]
26. Maluf, R.V.; Neves, J.C.S. Black holes with a cosmological constant in bumblebee gravity. *Phys. Rev. D* **2021**, *103*, 044002. [[CrossRef](#)]
27. Chen, S.; Wang, M.; Jing, J. Polarization effects in Kerr black hole shadow due to the coupling between photon and bumblebee field. *JHEP* **2020**, *7*, 54. [[CrossRef](#)]
28. Kanzi, S.; Sakallı, İ. Greybody radiation and quasinormal modes of Kerr-like black hole in Bumblebee gravity model. *Eur. Phys. J. C* **2021**, *81*, 501. [[CrossRef](#)]
29. Liu, C.; Ding, C.; Jing, J. Thin accretion disk around a rotating Kerr-like black hole in Einstein–bumblebee gravity model. *arXiv* **2019**, arXiv:1910.13259.
30. Güllü, İ.; Övgün, A. Schwarzschild-like black hole with a topological defect in bumblebee gravity. *Ann. Phys.* **2022**, *436*, 168721. [[CrossRef](#)]
31. Gomes, D.A.; Maluf, R.V.; Almeida, C.A.S. Thermodynamics of Schwarzschild-like black holes in modified gravity models. *Ann. Phys.* **2020**, *418*, 168198. [[CrossRef](#)]
32. Kanzi, S.; Sakallı, İ. Reply to “Comment on ‘Greybody radiation and quasinormal modes of Kerr-like black hole in Bumblebee gravity model’”. *Eur. Phys. J. C* **2022**, *82*, 93. [[CrossRef](#)]
33. Maluf, R.V.; Muniz, C.R. Comment on “Greybody radiation and quasinormal modes of Kerr-like black hole in Bumblebee gravity model”. *Eur. Phys. J. C* **2022**, *82*, 94. [[CrossRef](#)]
34. Jha, S.K.; Aziz, S.; Rahaman, A. Study of Einstein-bumblebee gravity with Kerr-Sen-like solution in the presence of a dispersive medium. *Eur. Phys. J. C* **2022**, *82*, 106. [[CrossRef](#)]
35. Ding, C.; Chen, X.; Fu, X. Einstein-Gauss-Bonnet gravity coupled to bumblebee field in four dimensional spacetime. *Nucl. Phys. B* **2022**, *975*, 115688. [[CrossRef](#)]
36. Jiang, R.; Lin, R.H.; Zhai, X.H. Superradiant instability of a Kerr-like black hole in Einstein-bumblebee gravity. *Phys. Rev. D* **2021**, *104*, 124004. [[CrossRef](#)]
37. Övgün, A.; Jusufi, K.; Sakallı, İ. Exact traversable wormhole solution in bumblebee gravity. *Phys. Rev. D* **2019**, *99*, 024042. [[CrossRef](#)]
38. Övgün, A.; Jusufi, K.; Sakallı, İ. Gravitational lensing under the effect of Weyl and bumblebee gravities: Applications of Gauss–Bonnet theorem. *Ann. Phys.* **2018**, *399*, 193–203. [[CrossRef](#)]
39. Xu, R.; Liang, D.; Shao, L. Bumblebee Black Holes in Light of Event Horizon Telescope Observations. *Astrophys. J.* **2023**, *945*, 148. [[CrossRef](#)]
40. Xu, R.; Liang, D.; Shao, L. Static spherical vacuum solutions in the bumblebee gravity model. *Phys. Rev. D* **2023**, *107*, 024011. [[CrossRef](#)]
41. Ding, C.; Shi, Y.; Chen, J.; Zhou, Y.; Liu, C.; Xiao, Y. Rotating BTZ-like black hole and central charges in Einstein-bumblebee gravity. *arXiv* **2023**, arXiv:2302.01580.
42. Ding, C.; Chen, X. Slowly rotating Einstein-bumblebee black hole solution and its greybody factor in a Lorentz violation model. *Chin. Phys. C* **2021**, *45*, 025106. [[CrossRef](#)]
43. Oliveira, R.; Dantas, D.M.; Almeida, C.A.S. Quasinormal frequencies for a black hole in a bumblebee gravity. *EPL* **2021**, *135*, 10003. [[CrossRef](#)]
44. Jha, S.K.; Rahaman, A. Bumblebee gravity with a Kerr-Sen-like solution and its Shadow. *Eur. Phys. J. C* **2021**, *81*, 345. [[CrossRef](#)]
45. Wang, Z.; Chen, S.; Jing, J. Constraint on parameters of a rotating black hole in Einstein-bumblebee theory by quasi-periodic oscillations. *Eur. Phys. J. C* **2022**, *82*, 528. [[CrossRef](#)]
46. Khodadi, M. Magnetic reconnection and energy extraction from a spinning black hole with broken Lorentz symmetry. *Phys. Rev. D* **2022**, *105*, 023025. [[CrossRef](#)]
47. Kuang, X.M.; Övgün, A. Strong gravitational lensing and shadow constraint from M87\* of slowly rotating Kerr-like black hole. *Ann. Phys.* **2022**, *447*, 169147. [[CrossRef](#)]
48. Jha, S.K.; Rahaman, A. Superradiance scattering off Kerr-like black hole and its shadow in the bumblebee gravity with noncommutative spacetime. *Eur. Phys. J. C* **2022**, *82*, 728. [[CrossRef](#)]
49. Liu, W.; Fang, X.; Jing, J.; Wang, J. QNMs of slowly rotating Einstein–Bumblebee black hole. *Eur. Phys. J. C* **2023**, *83*, 83. [[CrossRef](#)]
50. Khodadi, M.; Lambiase, G.; Mastrototaro, L. Spontaneous Lorentz symmetry breaking effects on GRBs jets arising from neutrino pair annihilation process near a black hole. *arXiv* **2023**, arXiv:2302.14200.
51. Turner, E.L. Gravitational lensing limits on the cosmological constant in a flat universe. *Astrophys. J. Lett.* **1990**, *365*, L43. [[CrossRef](#)]
52. Bartelmann, M.; Schneider, P. Weak gravitational lensing. *Phys. Rep.* **2001**, *340*, 291–472. [[CrossRef](#)]
53. Sauer, T. A brief history of gravitational lensing. *Einstein Online Band* **2010**, *4*, 3–1005.
54. Bartelmann, M. Gravitational Lensing. *Class. Quant. Grav.* **2010**, *27*, 233001. [[CrossRef](#)]
55. Sultana, J.; Kazanas, D. Bending of light in modified gravity at large distances. *Phys. Rev. D* **2012**, *85*, 081502. [[CrossRef](#)]

56. Rindler, W.; Ishak, M. Contribution of the cosmological constant to the relativistic bending of light revisited. *Phys. Rev. D* **2007**, *76*, 043006. [[CrossRef](#)]
57. Ishak, M.; Rindler, W.; Dossett, J. More on Lensing by a Cosmological Constant. *Mon. Not. R. Astron. Soc.* **2010**, *403*, 2152–2156. [[CrossRef](#)]
58. Bhattacharya, A.; Panchenko, A.; Scalia, M.; Cattani, C.; Nandi, K.K. Light bending in the galactic halo by Rindler-Ishak method. *JCAP* **2010**, *9*, 4. [[CrossRef](#)]
59. Bhattacharya, A.; Garipova, G.M.; Laserra, E.; Bhadra, A.; Nandi, K.K. The Vacuole Model: New Terms in the Second Order Deflection of Light. *JCAP* **2011**, *2*, 28. [[CrossRef](#)]
60. Cattani, C.; Scalia, M.; Laserra, E.; Bochicchio, I.; Nandi, K.K. Correct light deflection in Weyl conformal gravity. *Phys. Rev. D* **2013**, *87*, 047503. [[CrossRef](#)]
61. Heydari-Fard, M.; Mojahed, S.; Rokni, S.Y. Light bending in Reissner-Nordstrom-de Sitter black hole by Rindler-Ishak method. *Astrophys. Space Sci.* **2014**, *351*, 251–253. [[CrossRef](#)]
62. Fernando, S.; Meadows, S.; Reis, K. Null trajectories and bending of light in charged black holes with quintessence. *Int. J. Theor. Phys.* **2015**, *54*, 3634–3653. [[CrossRef](#)]
63. Ali, M.S.; Bhattacharya, S. Light bending, static dark energy, and related uniqueness of Schwarzschild–de Sitter spacetime. *Phys. Rev. D* **2018**, *97*, 024029. [[CrossRef](#)]
64. Seçuk, M.H.; Delice, Ö. Bending of light from Reissner–Nordström–de Sitter-monopole black hole. *Eur. Phys. J. Plus* **2020**, *135*, 610. [[CrossRef](#)]
65. Heydari-Fard, M.; Sepangi, H.R. Bending of light in novel 4D Gauss-Bonnet-de Sitter black holes by the Rindler-Ishak method. *EPL* **2021**, *133*, 50006. [[CrossRef](#)]
66. Mangut, M.; Gürsel, H.; Sakallı, İ. Gravitational lensing in Kerr–Newman anti de Sitter spacetime. *Astropart. Phys.* **2023**, *144*, 102763.
67. He, G.; Zhou, X.; Feng, Z.; Mu, X.; Wang, H.; Li, W.; Pan, C.; Lin, W. Gravitational deflection of massive particles in Schwarzschild-de Sitter spacetime. *Eur. Phys. J. C* **2020**, *80*, 835. [[CrossRef](#)]
68. Maldacena, J.M.; Strominger, A. Black hole grey body factors and d-brane spectroscopy. *Phys. Rev. D* **1997**, *55*, 861–870. [[CrossRef](#)]
69. Cvetič, M.; Larsen, F. Grey body factors for rotating black holes in four-dimensions. *Nucl. Phys. B* **1997**, *506*, 107–120. [[CrossRef](#)]
70. Harmark, T.; Natario, J.; Schiappa, R. Greybody Factors for d-Dimensional Black Holes. *Adv. Theor. Math. Phys.* **2010**, *14*, 727–794. [[CrossRef](#)]
71. Sakallı, İ.; Kanzi, S. Topical Review: Greybody factors and quasinormal modes for black holes in various theories—Fingerprints of invisibles. *Turk. J. Phys.* **2022**, *46*, 51–103. [[CrossRef](#)]
72. Sakallı, İ.; Aslan, O.A. Absorption cross-section and decay rate of rotating linear dilaton black holes. *Astropart. Phys.* **2016**, *74*, 73–78. [[CrossRef](#)]
73. Sakallı, İ. Analytical solutions in rotating linear dilaton black holes: Resonant frequencies, quantization, greybody factor, and Hawking radiation. *Phys. Rev. D* **2016**, *94*, 084040. [[CrossRef](#)]
74. Hawking, S.W. Particle Creation by Black Holes. *Commun. Math. Phys.* **1975**, *43*, 199–220; Erratum in *Commun. Math. Phys.* **1976**, *46*, 206. [[CrossRef](#)]
75. Hawking, S.W. Black hole explosions. *Nature* **1974**, *248*, 30–31. [[CrossRef](#)]
76. Bardeen, J. M.; Carter, B.; Hawking, S. W. The Four laws of black hole mechanics. *Commun. Math. Phys.* **1973**, *31*, 161–170. [[CrossRef](#)]
77. Ngampitipan, T.; Boonserm, P. Bounding the Greybody Factors for Non-rotating Black Holes. *Int. J. Mod. Phys. D* **2013**, *22*, 1350058. [[CrossRef](#)]
78. Boonserm, P.; Ngampitipan, T.; Wongjun, P. Greybody factor for black string in dRGT massive gravity. *Eur. Phys. J. C* **2019**, *79*, 330. [[CrossRef](#)]
79. Boonserm, P. Rigorous bounds on Transmission, Reflection, and Bogoliubov coefficients. *arXiv* **2009**, arXiv:0907.0045.
80. Boonserm, P.; Visser, M. Transmission probabilities and the Miller-Good transformation. *J. Phys. A* **2009**, *42*, 045301. [[CrossRef](#)]
81. Oshita, N. Thermal Ringdown of a Kerr Black Hole: Overtone Excitation, Fermi-Dirac Statistics and Greybody Factor. *arXiv* **2022**, arXiv:2208.02923
82. Cardoso, V.; Miranda, A.S.; Berti, E.; Witek, H.; Zanchin, V.T. Geodesic stability, Lyapunov exponents and quasinormal modes. *Phys. Rev. D* **2009**, *79*, 064016. [[CrossRef](#)]
83. Övgün, A. Black hole with confining electric potential in the scalar-tensor description of regularized 4-dimensional Einstein-Gauss-Bonnet gravity. *Phys. Lett. B* **2021**, *820*, 136517. [[CrossRef](#)]
84. Tuleganova, G.Y.; Karimov, R.K.; Izmailov, R.N.; Potapov, A.A.; Bhadra, A.; Nandi, K.K. Gravitational time advancement effect in Bumblebee gravity for Earth bound systems. *Eur. Phys. J. Plus* **2023**, *138*, 94. [[CrossRef](#)]
85. Schutz, B.F. *A First Course in General Relativity*; Cambridge University Press: London, UK, 1985.
86. Wald, R.M. *General Relativity*; Chicago University Press: New York, NY, USA, 1984.
87. Gurtug, O.; Mangut, M.; Halilsoy, M. Gravitational Lensing in Rotating and Twisting Universes. *Astropart. Phys.* **2021**, *128*, 102558. [[CrossRef](#)]
88. Fricke, T.T.; Smith-Lefebvre, N.D.; Abbott, R.; Adhikari, R.; Dooley, K.L.; Evans, M.; Fritschel, P.; Frolov, V.V.; Kawabe, K.; Kissel, J.S.; et al. DC readout experiment in Enhanced LIGO. *Class. Quant. Grav.* **2012**, *29*, 065005. [[CrossRef](#)]

89. Kokkotas, K.D.; Schmidt, B.G. Quasinormal modes of stars and black holes. *Living Rev. Rel.* **1999**, *2*, 2. [[CrossRef](#)]
90. Leung, P.T.; Liu, Y.T.; Suen, W.M.; Tam, C.Y.; Young, K. Perturbative approach to the quasinormal modes of dirty black holes. *Phys. Rev. D* **1999**, *59*, 044034. [[CrossRef](#)]
91. Daghighi, R.G.; Green, M.D. Validity of the WKB Approximation in Calculating the Asymptotic Quasinormal Modes of Black Holes. *Phys. Rev. D* **2012**, *85*, 127501. [[CrossRef](#)]
92. Decanini, Y.; Folacci, A.; Raffaelli, B. Unstable circular null geodesics of static spherically symmetric black holes, Regge poles, and quasinormal frequencies. *Phys. Rev. D* **2010**, *81*, 104039. [[CrossRef](#)]
93. Giri, S.; Nandan, H.; Joshi, L.K.; Maharaj, S.D. Geodesic stability and quasinormal modes of non-commutative Schwarzschild black hole employing Lyapunov exponent. *Eur. Phys. J. Plus* **2022**, *137*, 181. [[CrossRef](#)]
94. Bhar, P.; Rej, P. Stable and self-consistent charged gravastar model within the framework of  $f(R, T)$  gravity. *Eur. Phys. J. C* **2021**, *81*, 763. [[CrossRef](#)]

**Disclaimer/Publisher's Note:** The statements, opinions and data contained in all publications are solely those of the individual author(s) and contributor(s) and not of MDPI and/or the editor(s). MDPI and/or the editor(s) disclaim responsibility for any injury to people or property resulting from any ideas, methods, instructions or products referred to in the content.